Proceedings of 2024 IEEE
International Conference on Mechatronics and Automation
August 4 - 7, Tianjin, China

Motion Control of A Noval Bipedal Wheeled Robot:VC-I

Yi Wang, Yong Ding

Department of Automation
University of Science and Technology of China
443 Huangshan street,HeFei, China
{*wangyi0114& yding1111*}@mail.ustc.edu.cn

Yong Wang*

Department of Automation
University of Science and Technology of China
443 Huangshan street, HeFei, China
* *Corresponding author:*{*yongwang*}@ustc.edu.cn

2024 IEEE International Conference on Mechatronics and Automation (ICMA) | 979-8-3503-8807-7/24/$31.00 ©2024 IEEE | DOI: 10.1109/ICMA61710.2024.10632974

***Abstract*—Although the integration of wheeled and legged functionalities in robot designs, known as wheel-legged systems, enables operation across diverse environments, the demand for handling increasingly complex tasks necessitates wheel-leg systems equipped with a broader array of movement capabilities. In this paper, we have developed and implemented a motion control system on a novel tandem bipedal wheeled robot named VC-I. Within this system, addressing the robot's inherent static instability and the dynamic characteristics of its model, we have adopted the State-Dependent Riccati Equation (SDRE) method as the robot's balance controller. Additionally, tailored to meet the demands of specific tasks, we have designed controllers that manage a range of functions, including attitude angle and jumping capabilities, thereby enhancing the robot's operational versatility and effectiveness in varied environments. In conclusion, the effectiveness of the designed control system was validated through a comprehensive series of simulations and real-world experiments, confirming its viability and performance.**

Index Terms*—Bipedal wheeled robot, Motion control, State-Dependent Riccati Equation(SDRE)

Fig. 1: VC-I

I. Introduction

As a hybrid system that combines the advantages of wheeled robots with low energy consumption [1] and legged robots with strong adaptability [2] to complex environments, wheel-legged robots [3] [4] offer broad application prospects. The bipedal wheeled system [5] [6] [7] has the potential to explore more terrains in a miniaturized form due to its compact structure. However, to fully leverage the advantages of both wheeled and legged robots, it is essential for the robot to possess more flexible movement patterns. In addition, the under-actuated characteristics and complex structure of the bipedal wheeled system itself pose challenges to the control of its balance and other functions. In this work, we have designed and deployed a control system on a novel tandem bipedal wheeled robot, employing a nonlinear approach for balance control, and verified the effectiveness of the system through a series of simulations and real machine tests.

A. Related Work

In the realm of bipedal wheeled robots, key developments include Boston Dynamics' 'Handle' in 2017 [8]. While it represented notable innovation, the comprehensive technical details were not fully disclosed. ETH Zurich's 'Ascento' in 2019 [9], and Tencent's 'Ollie' in 2021 [10], furthered the field with advanced mobility features like dynamic jumping and somersaults, marking progressive enhancements in design and functionality.

Despite progress, a primary limitation lies in the mechanical design, where most robots move similarly to wheeled models, with legs mainly used for simple height adjustments. For instance, 'Ascento' relies only on hip joint motors and a four-bar linkage mechanism for its legged actions, resulting a limited range of joint motion. This design restricts the robots' ability to perform more complex locomotion patterns, such as mimicking human gait, which necessitates a broader spectrum of active degrees of freedom within the leg structure. However, enhancing the leg structure for increased mobility typically results in added mass, introducing higher inertia and diminishing control precision.

System control also faces significant challenges due to static stability issues. Although Linear Quadratic Regulator (LQR) [11] [12] methods have been applied with success, they struggle with accuracy when faced with model adjustments due to height changes and linearization errors. Meanwhile, nonlinear strategies like Input-Dependent Approximate Passivity-based

Control (IDA-PBC) [13] are promising but their complexity hampers wide use.

The State-Dependent Riccati Equation (SDRE) [14] [15] offers a more straightforward approach, efines LQR for handling nonlinear systems, integrating simplicity and adaptability. It utilizes the State-Dependent Coefficient (SDC) technique for precise, task-specific adjustments, and stands out for its ability to modify coefficient structure based on specific needs, providing a viable solution for complex control scenarios.

B. Contribution

The principal contribution of this article is the design and deployment of a comprehensive control system on a novel bipedal wheeled robot. This system employs the State-Dependent Riccati Equation (SDRE) method for balance control, tailored specifically to address the dynamic characteristics of the system. Furthermore, it includes controllers designed for functionalities such as jumping and posture angle adjustment, which are developed in accordance with the system's mechanical structure and task requirements. The effectiveness of this control system has been successfully validated through both simulations and real-world experiments.

II. Dynamic Model

A. Mechanical Structure

Fig. 1 showcases a novel bipedal wheeled robot with legs on driven wheels and a floating-base torso holding most electronics. The design's purpose centers on enhancing the robot's degrees of freedom and joint mobility. To achieve this, each leg is equipped with independently controlled hip and knee joints, each powered by dedicated motors.

To improve agility and optimize load distribution, the robot's knee joint is actuated by a motor mounted on the torso, connected via synchronous belts. This design decision in Fig. 2 diverges from the linkage mechanisms employed in some robots, offering our model an increased range of joint motion and reducing the mass of the legs. Moreover, the synchronous belt drive system inherently possesses shock absorption capabilities, which are essential for damping shock waves caused by sudden impacts, thus protecting the transmission components and maintaining the robot's structural integrity.

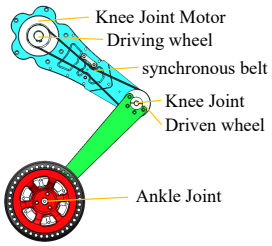

Fig. 2: Leg structure

This leg configuration enables the system to support a wide range of motion modes, such as free rotation of the torso, flexing of the leg structure both towards and away from the forward direction, and enhanced adaptability to impacts from actions like jumping.

B. Modeling

The configuration of this system allows upper body control to be decoupled from balance control. This separation obviates the necessity for full-body coordination, thereby markedly diminishing the computational burden involved in real-time control operations. Additionally, considering the leg's mass is negligible compared to the other part, its dynamic effects are considered minimal and are excluded from the model. Thus, the robot is modeled as a wheeled inverted pendulum (WIP), shown in Fig. 3, with its upper part represented as a virtual pole.

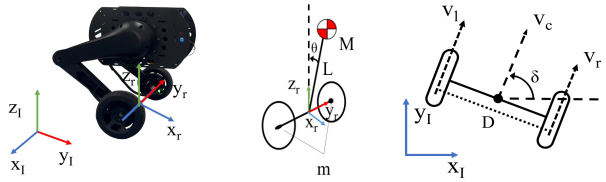

(a) (b) (c)

Fig. 3: Simplify the system into a wheeled inverted pendulum system and a two-wheel differential system

According to the Newton-Euler method, the dynamic model of the WIP is given by:

$$\begin{aligned}(M+m)\ddot{x} + mL\ddot{\theta}\cos\theta - mL\dot{\theta}^2\sin\theta + B\dot{x} = u \\ (I+mL^2)\ddot{\theta} + ml\ddot{x}\cos\theta - mgL\sin\theta = 0\end{aligned} \tag{1}$$

where M and m represent the masses of the virtual pole and the wheel respectively. L denotes the length from the center of mass of the virtual pole to the wheel axis; θ represents the inclination angle between the virtual pole and the vertical direction, named virtual angle; x is the displacement along the x-direction of the system; u is the control input, which in this system corresponds to the torque τ of the wheel motors; B is the coefficient of friction between the tire and the ground.

To compare control methods in later simulations, the system model is approximated and linearized near the equilibrium point $\theta = 0$ as:

$$\dot{x} = Ax + Bu \tag{2}$$

where $x = \begin{bmatrix} x & \theta & \dot{x} & \dot{\theta} \end{bmatrix}^T$ is the state variable and

$$A = \begin{bmatrix} 0 & 0 & 1 & 0 \\ 0 & 0 & 0 & 1 \\ 0 & a_{11} & a_{12} & 0 \\ 0 & a_{21} & a_{22} & 0 \end{bmatrix}, \quad B = \begin{bmatrix} 0 \\ 0 \\ b_1 \\ b_2 \end{bmatrix},$$

$$K = (M+m)\left[(I+mL^2) - m^2L^2\right],$$

$$a_{11} = \frac{m^2L^2g}{K}, \quad a_{12} = -\frac{B(I+mL^2)}{K}, \quad b_1 = \frac{I+mL^2}{K},$$

$$a_{21} = \frac{(M+m)mgL}{K}, \quad a_{22} = -\frac{BmL}{K}, \quad b_2 = \frac{mL}{K}$$

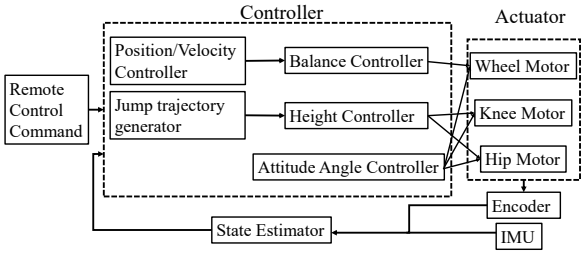

Fig. 4: System Control Framework

Since the system is approximated as a WIP modle, the virtual pole's length changes depending on the adjustment of the joint angle, and this motion relationship is captured using a single-leg Jacobian matrix as

$$\dot{\alpha} = J\dot{\beta} \tag{3}$$

where $\alpha = \begin{bmatrix} h & \theta \end{bmatrix}^T$ is the virtual pole's length and angle, $\beta = \begin{bmatrix} \theta_h & \theta_k \end{bmatrix}^T$, L_h, L_k are the hip and knee joint angles and the length of the thigh and calf of the robot.

$$\boldsymbol{J} = \begin{bmatrix} 0 & -\frac{L_h L_k \sin\theta_k}{\left(L_h^2+2L_hL_k\cos\theta_k+L_k^2\right)^{\frac{1}{2}}} \\ 1 & \frac{L_k(L_k+L_h\cos\theta_k)}{L_h^2+2L_hL_k\cos\theta_k+L_k^2} \end{bmatrix}$$

III. Control

Fig. 4 illustrates the system control framework, where inputs to the controller include both the system state, as estimated by sensors, and the remote control signal. These inputs collectively dictate the behavior of the system.

A. Balance Control

The core of the SDRE algorithm is to use the state-dependent coefficient(SDC) matrix to re-parameterize the nonlinear system and design the controller by solving the Riccati equation related to the system state.

First, parameterize the dynamics model of the WIP mentioned in eq. (1) by introducing the nonlinear system into a linear framework that incorporates a matrix of State-Dependent Coefficients .

$$\dot{x}(t) = A(x)x(t) + B(x)u(t) \tag{4}$$

The input vector u and the state variable x, consistent with definitions in eq. (2), allow the robot to track velocity and position, with yaw angle tracking designated for a separate, dedicated controller. The forms of the SDC matrices $A(x)$ and $B(x)$ are not unique. On the premise of ensuring pointwise controllability, relevant variables can be retained in SMC according to specific task requirements to achieve a trade-off between accuracy and computational efficiency.

Subsequently, at each time instant, this method treats the state-dependent coefficient matrix as a constant and computes the control actions by solving the LQ optimal control problem.

The statefeedback controller is obtained in the form

$$\begin{aligned} u(x) &= -K(x)x \\ K(x) &= -R^{-1}(x)B^T(x)P(x)x \end{aligned} \tag{5}$$

where P(x) is the unique, symmetric, positive-definite solution of the algebraic State-Dependent Riccati Equation

$$\begin{aligned} &P(x)A(x) + A^T(x)P(x) \\ &\quad - P(x)B(x)R^{-1}(x)B^T(x)P(x) + Q(x) = 0 \end{aligned} \tag{6}$$

with $Q(x)$ and $R(x)$ are weight matrices associated with the state variables and control inputs.

B. Motion Control

1) height control: In II-B, we manage height adjustments by tracking the virtual pole's length changes, sidestepping the complex nonlinear relation between torso height and joint angles. Thus, we use the force along the virtual pole, F_{des}, as our control variable, modulating it via a proportional derivative(PD) law based on remote signals or predefined trajectories.

$$F_{des} = k_p(H_{ref} - H) + k_d(\dot{H}_{ref} - \dot{H}) + G_{ref} \tag{7}$$

where k_p and k_d are the gains, and G_{ref} is feedforward compensation considering the torso's mass. Then we use the Jacobian matrix in eq. (3) to map torque to the joint space.

$$F_1 = J^T F_2 \tag{8}$$

where $F_1 = [T_h \ T_k]^T$ are the torque of the hip and knee joint motors and $F_2 = [F_{des} \ T_M]^T$ are the force along the virtual pole and the torque along the axis.

2) attitude angle control: The system decouples balance and yaw control by adopting a dual-wheel differential steering method. calculating steering torque via the same PD rule in eq.(7) and merging it with balance torque for output.

$$\tau_{des} = k_p(\dot{\delta}_{ref} - \dot{\delta}) + k_d(\ddot{\delta}_{ref} - \ddot{\delta}) \tag{9}$$

where $\dot{\delta} = \frac{\dot{x_l} - \dot{x_r}}{d}$ is the yaw angular velocity. The system's tracking of the torso's pitch angle and roll angle is also in

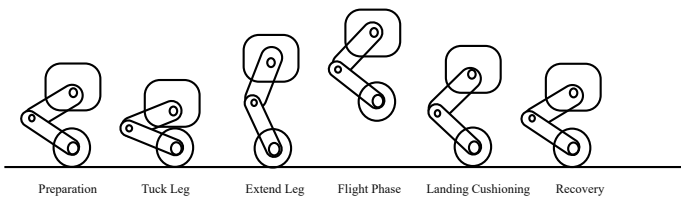

Fig. 5: Jumping Progress

3) jump control: In this system, jumping functionality is primarily achieved through a pre-defined leg height sequence activated by a remote command. This sequence, shown in

Fig. 5, is crafted through cubic spline interpolation to adjust height dynamically, starting with lowering the torso for jump preparation, then extending the legs for launch. During the airborne phase, balance control is turned off, and legs retract to maximize wheel height from the ground within motor torque limits. Landing triggers balance control reactivation for stable recovery. Simultaneously, the jump's trajectory, including time and height, is adjustable to meet diverse task requirements.

IV. Simulation And Experiments

A. Simulation

The control algorithms of the system were tested on the physical model built based on the Simscape module in Matlab. Additionally, for the design of the balance controller, we compared the designed SDRE controller with the sliding mode controller (SMC) of the cart inverted pendulum as described in [16].

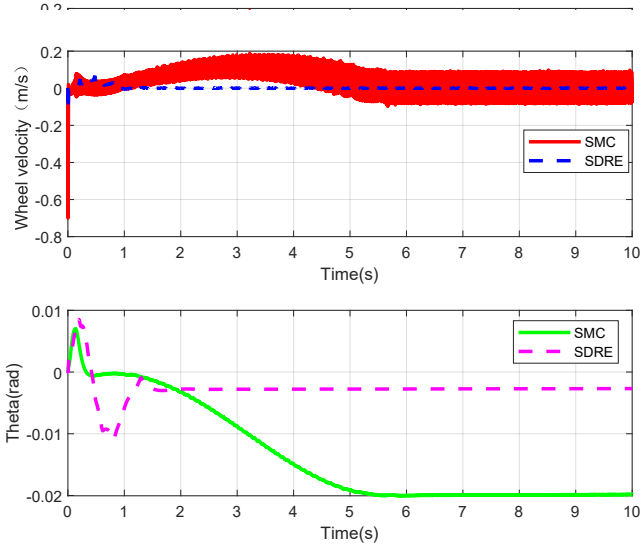

(b) Virtual angle θ

Fig. 6: Simulation

As shown in the Fig. 6, the system balance control simulation experiment results show that the SDRE can restore stability faster than the SMC, and at the same time, the virtual angle steady-state error is also smaller.

B. Experimental Setup

TABLE I: Parameters

Category	Parameters
Robot	M=15kg; m=2.8kg; R=0.08m; D=0.40m; l_1=0.26m; l_2=0.23m h_t=0.19m; 0.13m$\leq L \leq$0.57m
Controller	$Q_{val} = [10\ 100\ 200\ 10]$; $R_{val} = 0.8$;

Multiple experiments were conducted to assess the motion capabilities of the system. The mechanical parameters of the robot, as well as various control parameters, are listed in Table I.

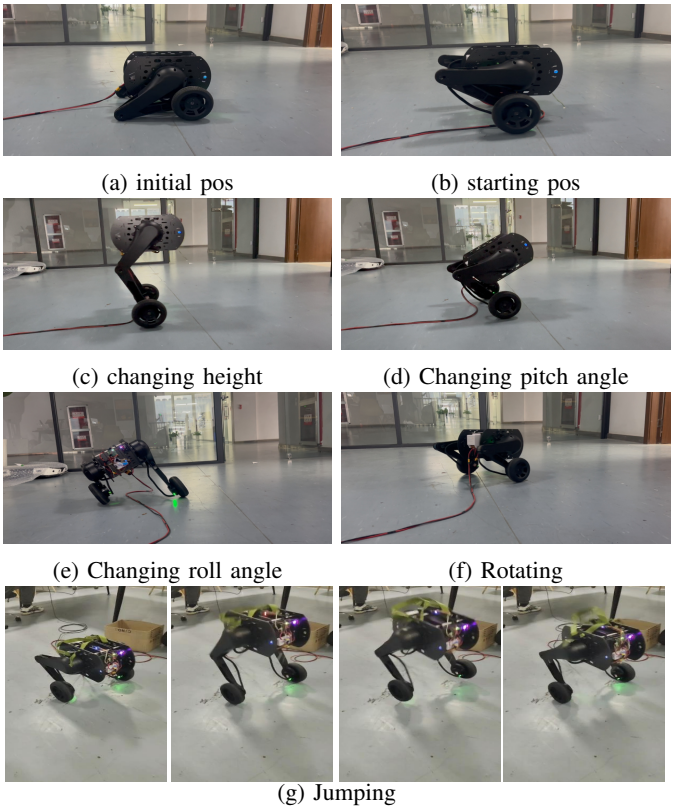

(a) initial pos (b) starting pos (c) changing height (d) Changing pitch angle (e) Changing roll angle (f) Rotating (g) Jumping

Fig. 7: Motion control experiment of bipedal wheeled robot prototype

In the table, M and m denote the weight of the whole upper part and the wheels, respectively. R is the wheel radius and D is the distance between wheels. h_t denotes the torso height. The height L dynamically calculated from motor angles and the lengths of calf l_1, thigh l_2, torso height h_t. To minimize computation, the weight matrix Q is chosen to be a diagonal matrix with with elements defined in Q_{val} and another weight matrix R_{val} is determined to be 0.8 based on experiments.

Control algorithms were simulated in MATLAB, then converted to C language. System employs LK-Tech's MG10015-V2 geared motors for joints and MF9025 direct-drive motors for hubs, with an STM32H7 as the main control board. IMU and encoder data inform body and joint position estimates, which, along with desired states, feed into the control module.

C. Experiments

We designed four experiments to test the stability of various motion control algorithms. Experimental images are presented in Fig. 7.

1) Balancing: The system's balance testing encompasses three key aspects: recovery from the initial to balanced position upon a start command (Fig.7a to 7b), maintaining stationary balance with a zero velocity command, and testing control algorithm robustness against disturbances from various directions.

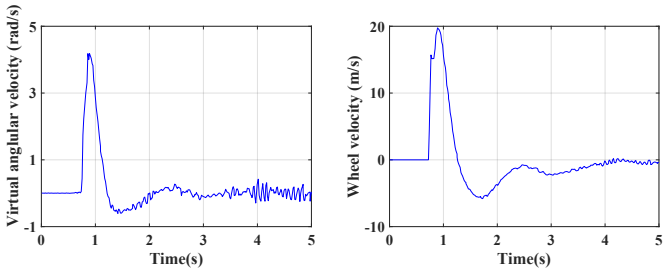

(a) Virtual angular velocity $\dot{\theta}$ (b) Wheel velocity $\dot{x}$

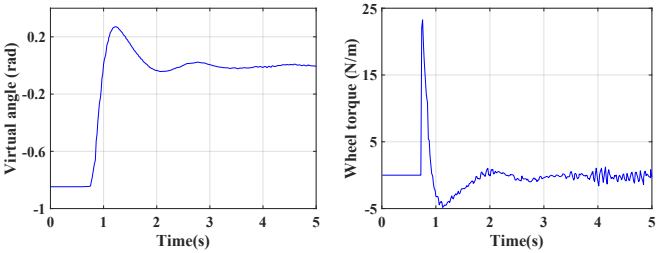

(c) Virtual angle θ (d) Torque input(Wheel) τ

Fig. 8: Start

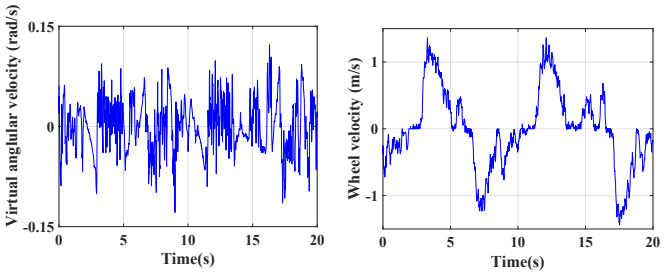

(a) Virtual angular velocity $\dot{\theta}$ (b) Wheel velocity $\dot{x}$

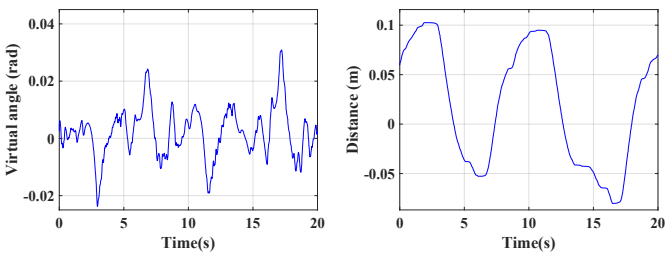

(c) Virtual angle θ (d) Distance x

Fig. 9: Balance

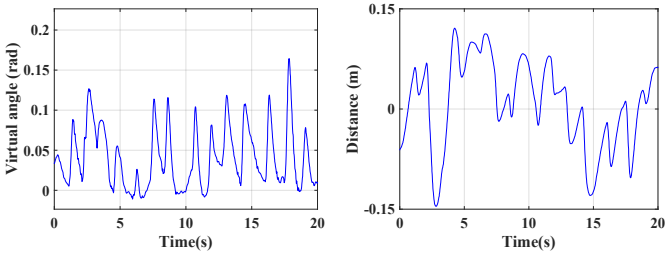

(a) Virtual angle θ (b) Distance x

Fig. 10: Disturbance

2) Changing Height: Test the system's response to different altitude commands (Fig. 7c) and verify whether the SDRE controller can maintain balance under varying altitude conditions.

3) Changing attitude angle: The experimental design for attitude angle control involves adjusting the system's pitch (Fig. 7d) and roll angles (Fig. 7e) and assessing yaw tracking performance(Fig. 7f). The implementation of these functions will help the robot achieve more complex tasks. For example, changes in the pitch angle of the torso can enhance the detection range of the vision system attached to it, and control of the roll angle is conducive to high-speed turning, etc.

4) Jumping: The system follows a predefined trajectory for height variation to perform a jumping action (Fig.7g). The evaluation involves assessing the system's responsiveness to high dynamic movements and its robustness in restoring balance control after landing.

D. Results

In this section, the experiments designed in the previous section were tested on the prototype and discussed.

1) Balancing: The system initiates its startup process from a 45° virtual angle upon receiving an activation command, quickly aligning to equilibrium position within $1s$ (Fig. 8c) and maintaining a stationary stance as depicted in Fig. 8b.

During stationary balance testing, the system's virtual angle stabilizes near zero with fluctuations within 1°, countered by wheel oscillations within a 5cm range (Figs. 9c and 9d), showcasing the controller's effectiveness in maintaining stillness.

In the balance control experiment's final stage, we applied external perturbations of varying magnitudes and directions to the system. As shown in Fig. 10a, within the range of disturbances that a normal adult male can impose, the system's virtual angle shifted. However, the virtual angle's deviation stayed below 12°, and system displacement was limited to 15cm (Figs. 10a and 10b), evidencing the system's capability to recover balance within acceptable offsets and demonstrating its robustness against external forces.

2) Changing Height: As demonstrated in Fig. 11, The system can adjust its height from 0.13m to 0.45m based on the reference signal while maintaining balance. Despite the mechanical design permitting adjustments from 0.13m to 0.57m, we limit the height to 0.45m to avoid issues with joint angle calculations caused by the system's legs becoming completely vertical.

3) Changing attitude angle: The first is the tracking experiment of the pitch angle. Despite the hip joint motor's ability for 360° rotation, practical factors like viewable range and circuit layout restrict the pitch angle within $\pm 40^\circ$. And experimental in Fig. 12 show the robot's excellent tracking performance to reference signals.

In the roll angle tracking experiment, the reference roll angle is restricted to $\pm 25^\circ$ to prevent the system rolling over. As illustrated in Fig. 13, The system can track reference angle, but restoring balance from large angles causes overshoot, primarily

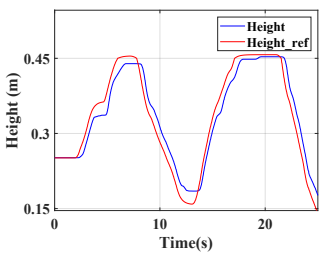

Fig. 11: Height

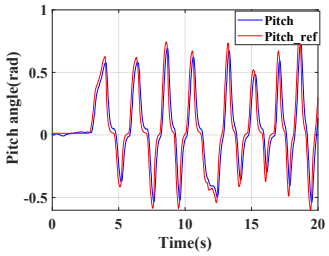

Fig. 12: Pitch

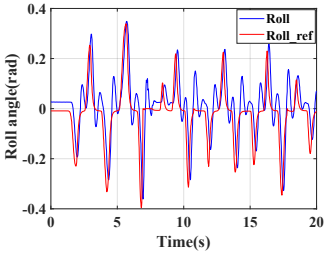

Fig. 13: Roll

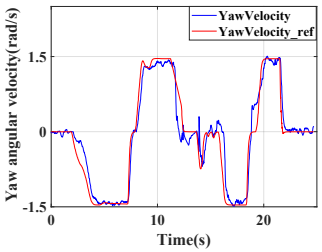

Fig. 14: Rotate

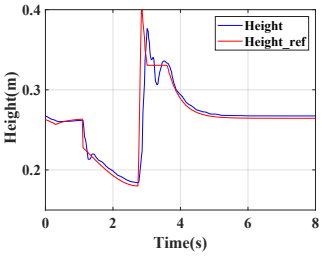

(a) Height

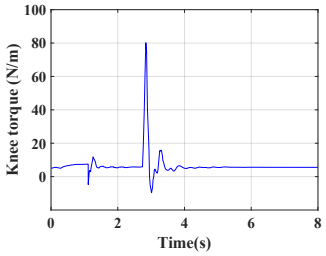

(b) Torque input(Knee)

Fig. 15: Jump

due to the synchronous belt drive's elasticity, which cushions leg impact with the ground.

Lastly, to avoid angle calculation problems from multi-turn rotations, we track yaw angular velocity instead of yaw angle. And system, shown in Fig. 14, allows precise and balanced tracking of yaw velocity, achieving up to $90°/s$ rotation speed in both directions.

4) Jumping: In the experiment, as shown in Fig. 15a, the system executed a jump command 1s after initiation, adjusting the torso height according to a predetermined trajectory. Leg extension began at 3s, achieving lift-off in just 0.1s. During the airborne phase, legs were further retracted to maximize wheel-ground clearance. The system smoothly landed at 4s, returning to the set height. This demonstrates the system's ability to accurately follow height changes, execute dynamic jumps, and maintain a 6-7cm clearance from the ground during flight.

V. Conclusion

In this research, we successfully deployed a control system on a novel tandem bipedal wheeled robot, fully leveraging its expanded range of motion and enhanced degrees of freedom. Utilizing the State-Dependent Riccati Equation (SDRE) approach for balance control, we effectively addressed the challenges posed by the model's time-variant nature. The robustness and functionality of our design were confirmed through simulations and rigorous prototype evaluations. However, the robot currently lacks environmental perception and complex task execution capabilities. To remedy this, we plan to address these limitations in future work by integrating sensory systems and advanced task management, aiming to enhance its navigation, collaboration, and practical application utility.

References

[1] A. De Luca, G. Oriolo, and M. Vendittelli, "Control of wheeled mobile robots: An experimental overview," *RAMSETE: articulated and mobile robotics for services and technologies*, pp. 181–226, 2002.

[2] J. Tenreiro Machado and M. Silva, "An overview of legged robots," in *International Symposium on Mathematical Methods in Engineering*, pp. 1–40, 2006.

[3] M. Bjelonic, V. Klemm, J. Lee, and M. Hutter, "A survey of wheeled-legged robots," in *Climbing and Walking Robots Conference*, pp. 83–94, Springer, 2022.

[4] Swiss-Mile. [Online]. Available: https://www.swiss-mile.com/.

[5] M. Wahde and J. Pettersson, "A brief review of bipedal robotics research," in *Proceedings of the 8th UK Mechatronics Forum International Conference (Mechatronics 2002)*, pp. 480–488, 2002.

[6] X. Li, H. Zhou, H. Feng, S. Zhang, and Y. Fu, "Design and experiments of a novel hydraulic wheel-legged robot (wlr)," in *2018 IEEE/RSJ International Conference on Intelligent Robots and Systems (IROS)*, pp. 3292–3297, IEEE, 2018.

[7] X. Liu, Y. Sun, S. Wen, K. Cao, Q. Qi, X. Zhang, H. Shen, G. Chen, J. Xu, and A. Ji, "Development of wheel-legged biped robots: A review," *Journal of Bionic Engineering*, pp. 1–28, 2024.

[8] Handle. [Online]. Available: https://www.bostondynamics.com/handle.

[9] V. Klemm, A. Morra, C. Salzmann, F. Tschopp, K. Bodie, L. Gulich, N. Küng, D. Mannhart, C. Pfister, M. Vierneisel, *et al.*, "Ascento: A two-wheeled jumping robot," in *2019 International Conference on Robotics and Automation (ICRA)*, pp. 7515–7521, IEEE, 2019.

[10] S. Wang, L. Cui, J. Zhang, J. Lai, D. Zhang, K. Chen, Y. Zheng, Z. Zhang, and Z.-P. Jiang, "Balance control of a novel wheel-legged robot: Design and experiments," in *2021 IEEE International Conference on Robotics and Automation (ICRA)*, pp. 6782–6788, IEEE, 2021.

[11] Z. Li, C. Yang, and L. Fan, *Advanced control of wheeled inverted pendulum systems*. Springer Science & Business Media, 2012.

[12] E. V. Kumar and J. Jerome, "Robust lqr controller design for stabilizing and trajectory tracking of inverted pendulum," *Procedia Engineering*, vol. 64, pp. 169–178, 2013.

[13] R. Ortega, M. W. Spong, F. Gómez-Estern, and G. Blankenstein, "Stabilization of a class of underactuated mechanical systems via interconnection and damping assignment," *IEEE transactions on automatic control*, vol. 47, no. 8, pp. 1218–1233, 2002.

[14] T. Çimen, "State-dependent riccati equation (sdre) control: A survey," *IFAC Proceedings Volumes*, vol. 41, no. 2, pp. 3761–3775, 2008.

[15] T. Çimen, "Systematic and effective design of nonlinear feedback controllers via the state-dependent riccati equation (sdre) method," *Annual Reviews in control*, vol. 34, no. 1, pp. 32–51, 2010.

[16] J. Liu, "Sliding mode control design and matlab simulation," in *the basic theory and design method*, Tsinghua University Press, 2012.